Student: Jean-Baptiste Sauvan
Supervisor: Gerhard Brandt September 2007

Search for Anomalous Single Top Quark Production in ep Collisions with the H1 Experiment

DESY Summer Student Program

-

Report

Abstract

A search for single top production using the H1 experiment is performed using the full amount of data collected between 1994 and 2007, corresponding to an integrated luminosity of 486pb^{-1}. The hadronic decay channel $t \rightarrow bW \hookrightarrow q\bar{q}$ is investigated. In a cut-based analysis, 123 data events are selected when the prediction for Standard Model processes is 119 ± 36 events. A multivariate likelihood analysis is also performed in addition to the cut-based analysis. The top signal contribution in each channel is then determined in a maximum-likelihood fit to the likelihood discriminator distributions. For the combination of the semi-leptonic and the hadronic channel, a cross-section for single top production of $\sigma = 0.02^{+0.05}_{0.03}$ pb at $\sqrt{s} = 320$ GeV is obtained. Exclusion limits for the single top cross-section of $\sigma < 0.123$ pb and for the anomalous coupling $\kappa_{tu\gamma} < 0.119$ are also set. Finally, we extend this analysis and set 95% CL limits in $\kappa_{tu\gamma}$–v_{tuZ} plane

1 Introduction

In ep collisions at the HERA collider, the production of single top quarks is kinematically possible due to the large centre–of–mass energy of $\sqrt{s} = 320$ GeV, which is well above the top production threshold. In the Standard Model, the dominant process for single top production at HERA is the charged current reaction $e^+p \to \bar{\nu}t\bar{b}X$ ($e^-p \to \nu\bar{t}bX$). This process has a tiny cross section of less than 1 fb and thus Standard Model top production is negligible. However, in several extensions of the Standard Model, the top quark is predicted to undergo flavour changing neutral current (FCNC) interactions, which could lead to a sizeable top production cross section. FCNC interactions are present in models which contain an extended Higgs sector, Supersymmetry, dynamical breaking of the electroweak symmetry or an additional symmetry. An observation of top quarks at HERA would therefore be an indication of physics beyond the Standard Model [1].

A FCNC vertex involving the direct coupling of the top quark to a light quark (u or c) and a gauge boson would lead to single top production, as illustrated in figure 1. The most general effective Lagrangian which describes FCNC top quark interactions involving electroweak bosons is

$$
\begin{aligned}
\mathcal{L}_{eff}^{FCNC} &= \sum_{U=u,c} \frac{ee_U}{2\Lambda}\kappa_{tU\gamma}\bar{t}\sigma_{\mu\nu}A^{\mu\nu}U \\
&+ \frac{g}{2\cos\theta_W}\bar{t}\left[\gamma_\mu(v_{tUZ} - a_{tUZ}\gamma^5)UZ^\mu + \frac{1}{2\Lambda}\kappa_{tUZ}\sigma_{\mu\nu}Z^{\mu\nu}U\right] \quad + \text{h.c.}\,, \qquad (1)
\end{aligned}
$$

where $\sigma_{\mu\nu} = (i/2)\,[\gamma^\mu, \gamma^\nu]$, θ_W is the Weinberg angle, e and g are the couplings to the gauge groups with $U(1)$ and $SU(2)$ symmetries respectively, e_U is the electric charge of up–type quarks, A^μ and Z^μ are the fields of the photon and the Z boson and Λ is the scale up to which the effective theory is assumed to be valid. The tensors $A^{\mu\nu}$ and $Z^{\mu\nu}$ are the field strength tensors of the photon and Z boson fields. By convention Λ is set equal to the top mass in the following, which we consider to be equal to 175 MeV. Because gauge invariance is required, only magnetic operators allow FCNC couplings of the top quark to a photon and an up–type quark $U = u, c$, denoted by $\kappa_{tU\gamma}$, while the non–vanishing Z mass allows both the magnetic coupling κ_{tUZ} and the vector and axial vector couplings to a Z boson and an up–type quark, denoted by v_{tUZ} and a_{tUZ}.

A search for single top production is performed in data collected between 1994 and 2007, corresponding to an integrated luminosity of $\mathcal{L} = 486$ pb^{-1}. We use both a cut-based search and a multivariate likelihood discriminator to extract the top signal (the simulation of the anomalous single top signal relies on an event generator: ANOTOP [2]) from the Standard Model background in the data. This analysis is only performed in the case where the W boson decays hadronically because the study of the semi-leptonic channel has already been done before [3]. Thanks to the likelihood discriminators, we can do a maximum-likelihood fit of the top contribution in the data, which allows us to set a limit on the cross-section for anomalous single top production, and on the magnetic coupling $\kappa_{tu\gamma}$ (when coupling v_{tuZ} is neglected). Finally, we extend the analysis into the whole $tu\gamma$–tuZ coupling plane by taking the v_{tuZ} coupling fully into account in the calculation of the cross-section $ep \to et \to ebW \to ebud$ [2].

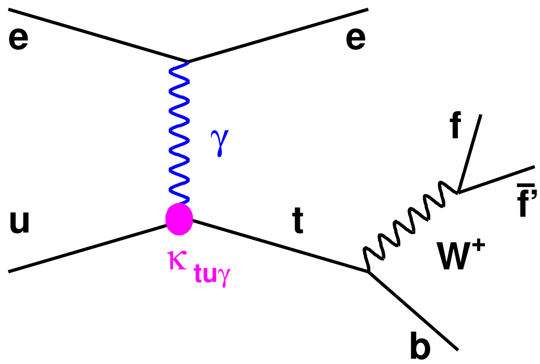

Figure 1: Anomalous single top production via a flavour changing neutral current interaction at HERA, with subsequent decays $t \to bW^+$ and $W^+ \to f\bar{f}'$.

2 Top search in the hadronic decay channel

First, a search for single top production is performed in the hadronic channel. The decay cascade $t \to bW \to bq\bar{q}'$ yields events with at least three jets with high transverse momenta. The main Standard Model background is the QCD production of high-P_T jets in photoproduction (simulated by PYTHIA generator), neutral current deep inelastic scattering (simulated by RAPGAP generator) and W production (simulated by EPVEC). The full HERA 1+2 data set is used. H1OO software is used as well as the Marana framework. All calibrations for jets and electro-magnetic particles are applied.

2.1 Pre-selection of multi-jets events

For the pre-selection of top candidates, only events with at least three jets are selected. All the jets must have a pseudorapidity range of $-0.5 < \eta_{jet} < 2.5$. Furthermore, the three highest-P_T jets must fulfill the following transverse momentum criteria : $P_T^{jet1} > 25$ GeV, $P_T^{jet2} > 20$ GeV, and $P_T^{jet3} > 15$ GeV. Additional jets are accepted if their tranverse momenta are larger than 4 Gev. In order to remove electrons that are mis-identified as hadronic jets, each jet is required to either have an energy fraction in the electromagnetic calorimeter of less than 90% of its total energy or a size in the $\eta - \Phi$ plane larger than 0.1.

In figure 2, control distributions for the multi-jet pre-selection are presented. The photoproduction (GP) and neutral current (NC and NCB) Monte Carlos, as well as the W production, represent the Standard Model Background, which is normalized to the luminosity. The shapes of the studied distributions are in reasonable agreement with the simulation. With these requirements, the pre-selected multi-jet sample contains 7445 data events, when the SM expected number of events is 8791 ± 2175 (see table 1). A theoretical error of 30% is assumed on the NC and GP; it is added in quadrature to the statistical error. The efficiency for single top production is 51%. This selection is also done for the HERA 1 period only, so that we can compare with Tab. 7.1 in [1]. Results in this case are shown in table 2.

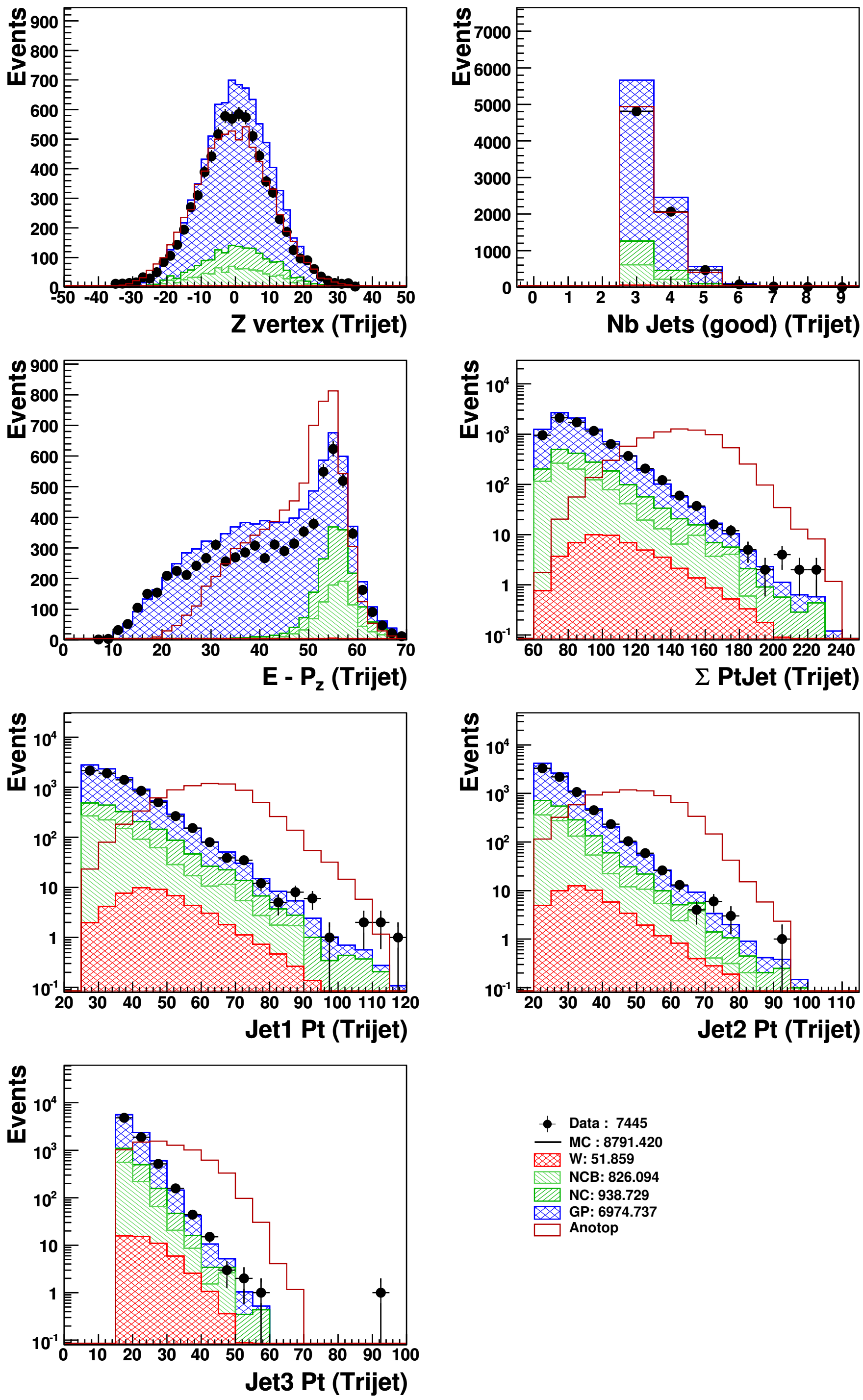

Figure 2: Control distributions of the multi-jet pre-selection. The top simulation is shown as red histogram, normalized to the same area as the Standard Model background. ($e^{\pm}p$ Data 94-07 486pb^{-1})

Hadronic channel	Data 94-07	SM	GP	NC	NCB	W prod.	ϵ_{top}
Multi-jet Pre-selection	7445	8791 ± 2175	6975	939	826	52	51%
High-E_t and W cand.	497	523.5 ± 115.6	357	94	53	19	42%
Top-candidates	123	141.1 ± 29.0	86	26	22	7	31%

Table 1: Observed and predicted events for the multi-jet pre-selection, the selection of multi-jet events with high-E_t and a W candidate, and top-candidate events selected in a cut-based analysis, for 1994-2007 period. Errors on the Standard Model correspond to a theoretical uncertainty of 30$\%$.

Hadronic channel	Data 94-00	SM	GP	NC	NCB	W prod.	ϵ_{top}
Multi-jet Pre-selection	1625	2000 ± 504	1620	223	145	12	51%
High-E_t and W cand.	118	113 ± 26	79.3	19.6	10.1	4.4	42%
Top-candidates	33	30.6 ± 6.4	19.0	6.0	4.0	1.5	31%

Table 2: Observed and predicted events for the multi-jet pre-selection, the selection of multi-jet events with high-E_t and a W candidate, and top-candidate events selected in a cut-based analysis, for 1994-2000 period. Errors on the Standard Model correspond to a theoretical uncertainty of 30$\%$.

2.2 Selection of events with high-E_T and a W candidate

To enhance a possible top signal relative to the QCD background, the phase space is further restricted to a region of higher jet transverse momenta. Furthermore, candidate events for top production are required to have the signature of a W boson in the event. The two highest-P_T jets must have transverse momenta $P_T^{jet1} > 40$ GeV and $P_T^{jet2} > 30$ GeV. In top events, the three highest-P_t jets correspond to the b-quark and to the quarks from the W decay. Due to the high top mass, a large amount of transverse energy is expected in events from top production; therefore, the total transverse energy ($\Sigma PtJet$ in figure 2) is required to be above 110 GeV.

As the top quark decays into a b-quark and a W boson, we need to identify these two decay products in the events we want to select. But it is not obvious which of the jets correspond to the $q\bar{q}'$ pair from the W decay, and which to the b-quark. The three highest-P_T jets are associated to the b-quark and to the hadronic decay of the Waccording to the following procedure:

- The two jets with an invariant mass closest to the W mass are assigned to the W decay products. The invariant mass of these two jets is denoted with $M\_W^{comb.}$.
- The remaining jet among the three highest-P_T jets is assigned to the b-quark from the top decay.

As a sign of a W boson in the event, one of the invariant masses of the different di-jet combinations must have a value close to the nominal W mass. To select events with potential W candidates, a window on $M\_W^{comb.}$ is set around the W mass:

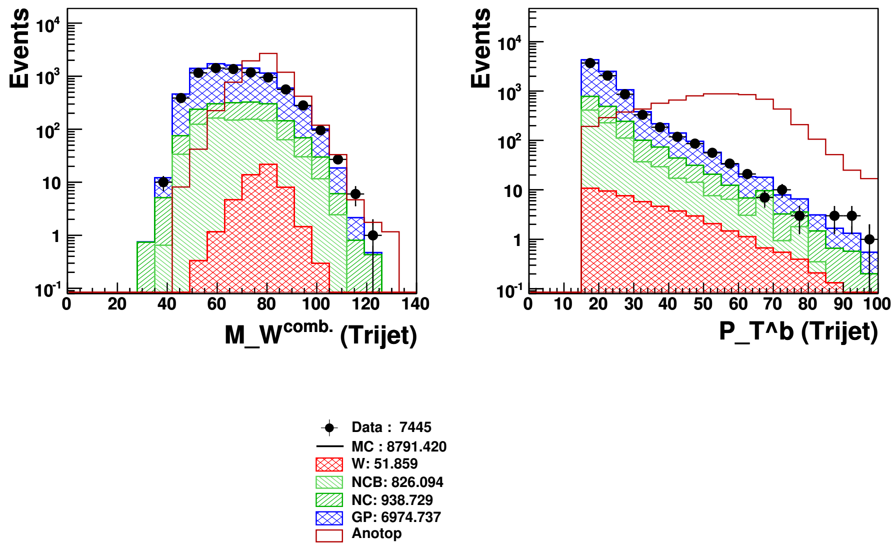

Figure 3: Control distributions of the multi-jet pre-selection used to identify the b-jet and the two jets from the W decay. ($e^{\pm}p$ Data 94-07 486pb^{-1})

$$65GeV < M\_W^{comb.} < 95GeV$$

The selection of multi-jets events with high E_T and a W candidate yields 497 events when the Standard Model expectation is 524 ± 116 events (see table 1). The efficiency for single top production is 42%. Distributions of the transverse momenta and pseudorapidities of the jets are displayed in figure 4. The shape of all distributions are in agreement with the Standard Model prediction.

2.3 Top search

Finally, in order to discriminate Top and QCD background in a better way, we use the distributions of three observables we didn't use before:

- P_T^b, the transverse momentum of the b-jet candidate.
- M_{jets}, the invariant mass of all selected jets in the event.
- $cos(\theta_W^{\star})$, the W decay angle. It is defined as the angle between the lower-P_T jet of the two jets assigned to the W decay in the W rest frame and the direction of the W in the top rest frame.

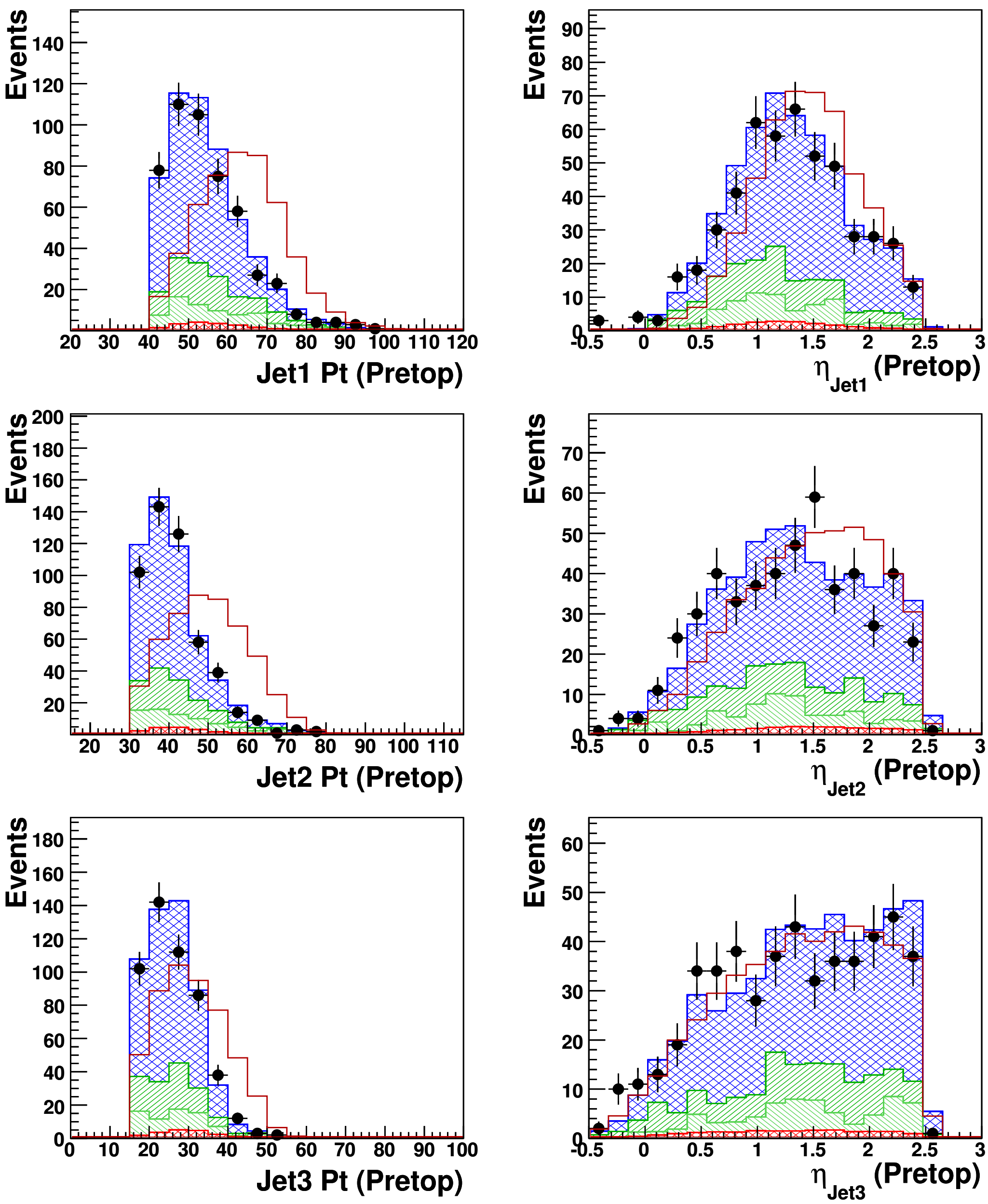

Figure 4: Distributions of the jet tranverse momemta and pseudorapidity for the selection of multi-jet events with high E_t and a W candidate. The top simulation is normalized to the same area as the Standard Model background. ($e^{\pm}p$ Data 94-07 486pb^{-1})

As can be seen in figure 5, all three observables exhibit a good discrimination between the top signal and the QCD background. We also plot these distributions for HERA 1 period only in 6, to be compared with Fig.5 in [1]).

The final selection of top candidates in the hadronic channel is performed using both a simple cut-based analysis and a likelihood analysis. First we discuss the selection cuts and the results of the cut-based analysis.

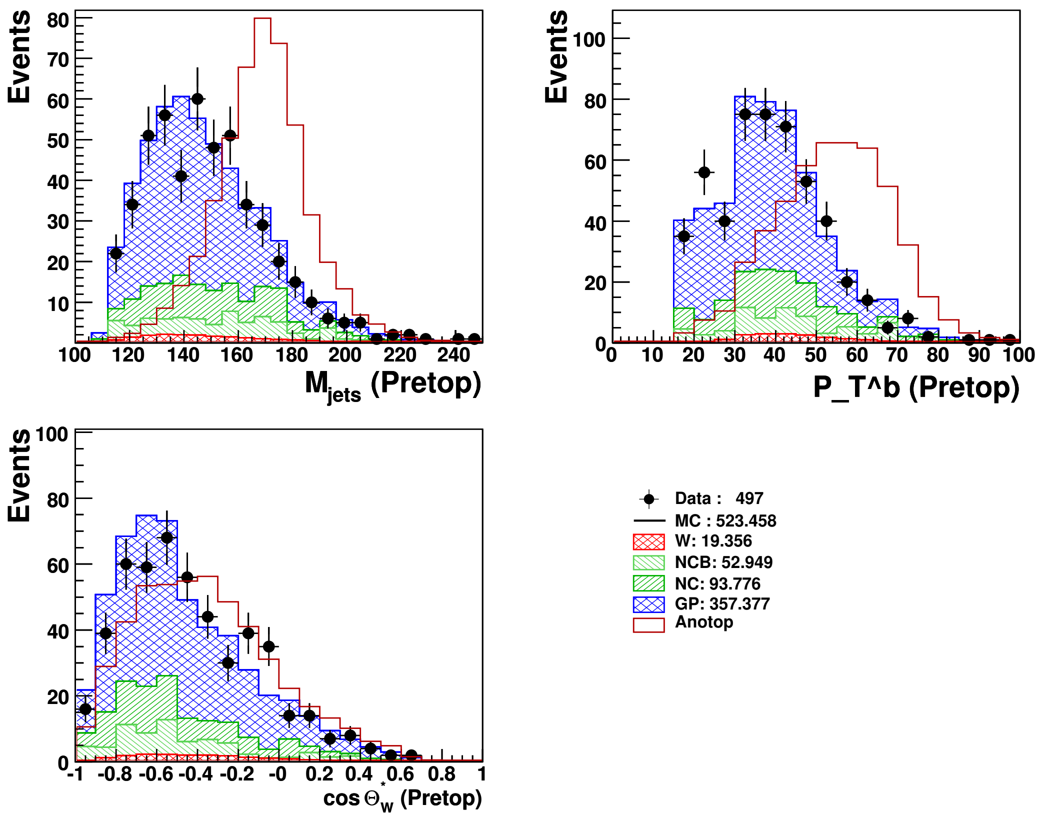

Figure 5: Distributions of the three observables used to discriminate the top signal from the Standard Model Background. The top simulation is normalized to the same area as the Standard Model background. ($e^{\pm}p$ HERA 1+2 94-07 486pb^{-1})

Table 3 shows the top selection cuts imposed on the three dicriminating observables. In the cut-based analysis, 123 data events are selected as top candidates. The number of observed data events agree with the Standard Model expectation of 141 ± 29 (see table 1). No excess of events as a signal of top production is observed. But more events in data and Monte Carlo sample are selected, compare to [1]. 33 events are selected in the data compare to 18 in [1], and 30.6 ± 6.4 in the Monte Carlo sample compare to $20.2 \pm 3,0$. This means that some cuts are not applied exactly in the same way. We didn't yet figure out where the differences are. In Appendix E in [1], five top candidates are selected; we compare in table 4 the differences between our analysis and [1] for these events.

Observables	Top selection cuts
Transverse momentum of b-candidate	$P_T^b > 40GeV$
W decay angle	$cos(\theta_W^\star) > -0.75$
Invariant mass of the jets	$150GeV < M_{jets} < 210GeV$

Table 3: Cuts used in the cut-based selection.

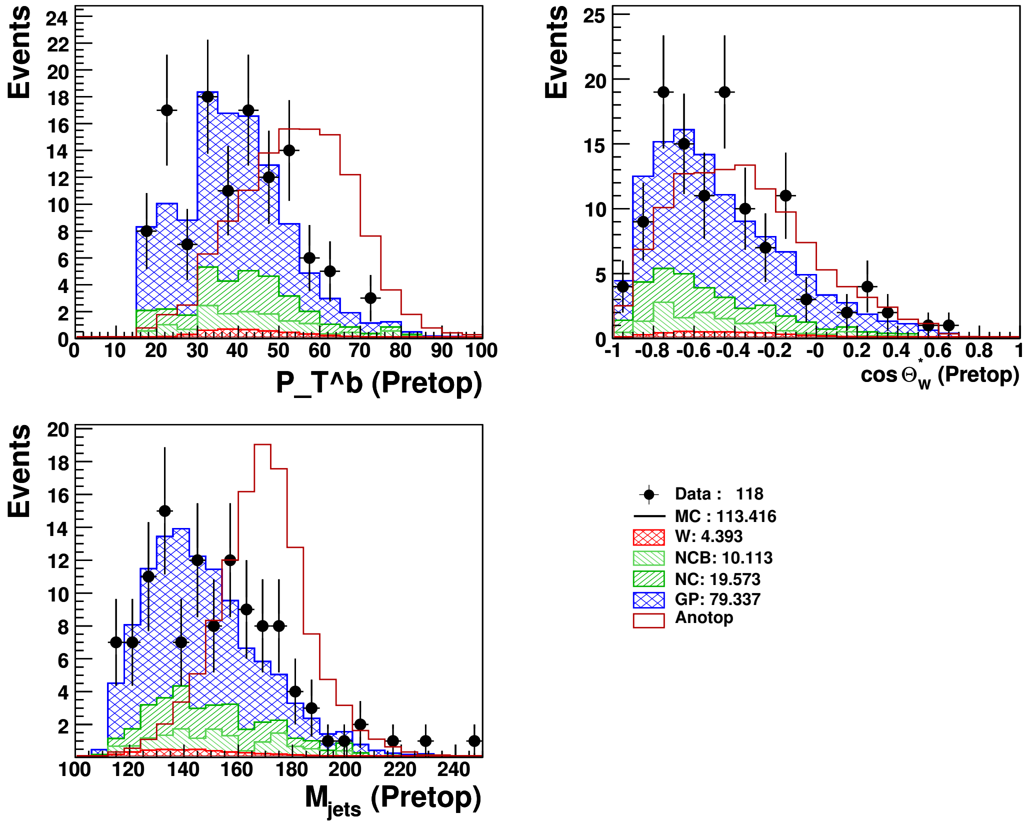

Figure 6: Distributions of the three observables used to discriminate the top signal from the Standard Model Background. The top simulation is normalized to the same area as the Standard Model background. ($e^{\pm}p$ HERA 1 94-00 118pb^{-1})

Run-Event	analysis	$P_T^{jet1,2,3}$	M_{jets}	$M_{2jet}^{W comb.}$
277152-17273	thesis	70,69,21 GeV	171 GeV	71 GeV
	here	not selected $P_T^{jet3} < 15$GeV		
271055-119291	thesis	70,60,22 GeV	174 GeV	81 GeV
	here	75,56,23 GeV	172 GeV	84 GeV
272940-46911	thesis	75,68,24 GeV	186 GeV	85 GeV
	here	85,60,22 GeV	182 GeV	83 GeV
278168-147146	thesis	63,43,23 GeV	181 GeV	70 GeV
	here	not selected $M_{jets} > 210$GeV		
274439-64676	thesis	68,42,36 GeV	180 GeV	75 GeV
	here	74,41,37 GeV	182 GeV	72 GeV

Table 4: Comparison of top candidates events in [1] and in our analysis.

The likelihood method is applied to combine the discriminating observables in a single likelihood discriminator and improve the sensitivity of the top selection. We use a multivariate likelihood method contained in the TMVA toolkit [5]. In a likelihood method, a decision is taken to classify an event as signal or background candidate on the basis of a single discriminator L. The measurements of n observables x_i (in our case the three observables presented above) for each event are combined in an n-dimensional vector of measurements $\mathbf{x} = (x_1, ..., x_n)$.The likelihood discriminator is then defined as:

$$L = \frac{P_{signal}(\mathbf{x})}{P_{signal}(\mathbf{x}) + P_{bkg}(\mathbf{x})}$$

where $P_{signal}(\mathbf{x})d^n x$ and $P_{bkg}(\mathbf{x})d^n x$ are the probabilities to produce a measurement $\mathbf{x}$ in a volume element $d^n x$ for a signal and background event, respectively.

By definition, the likelihood discriminator varies in the segment $[0, 1]$. Signal events tend to have values close to one, while background events tend to be close to zero. In the standard likelihood method, the joint probability density $P(\mathbf{x})$ for both signal and background events is approximated by the product of the one-dimensional probability density functions $p_i(x_i)$ for each single observable:

$$P(\mathbf{x}) = \prod_{i=1}^{n} p_i(x_i)$$

Technically, the probability densities functions $p_i(x_i)$ correspond to the normalized histograms of the discriminating observables x_i for the signal and background Monte Carlo samples.

The three observables in figure 5 serve as input to the likelihood analysis. We obtain the likelihood discriminator shown in figure 7. The electron and muon channels are taken from [3] and use a phase space density discriminator based on a range-search algorithm. The performance of the likelihood discriminator compared to a cut-based analysis is shown in table 5.

Hadronic channel	Data 94-07	SM	ϵ_{top}
Top cuts	123	119.0 ± 36.3	31%
Cut $L > 0.6$	136	142.6	30%
Cut $L > 0.8$	36	43.4	17%

Table 5: Summary of the observed and predicted number of events for the cut-based top analysis and for different cuts on the likelihood discriminator L.

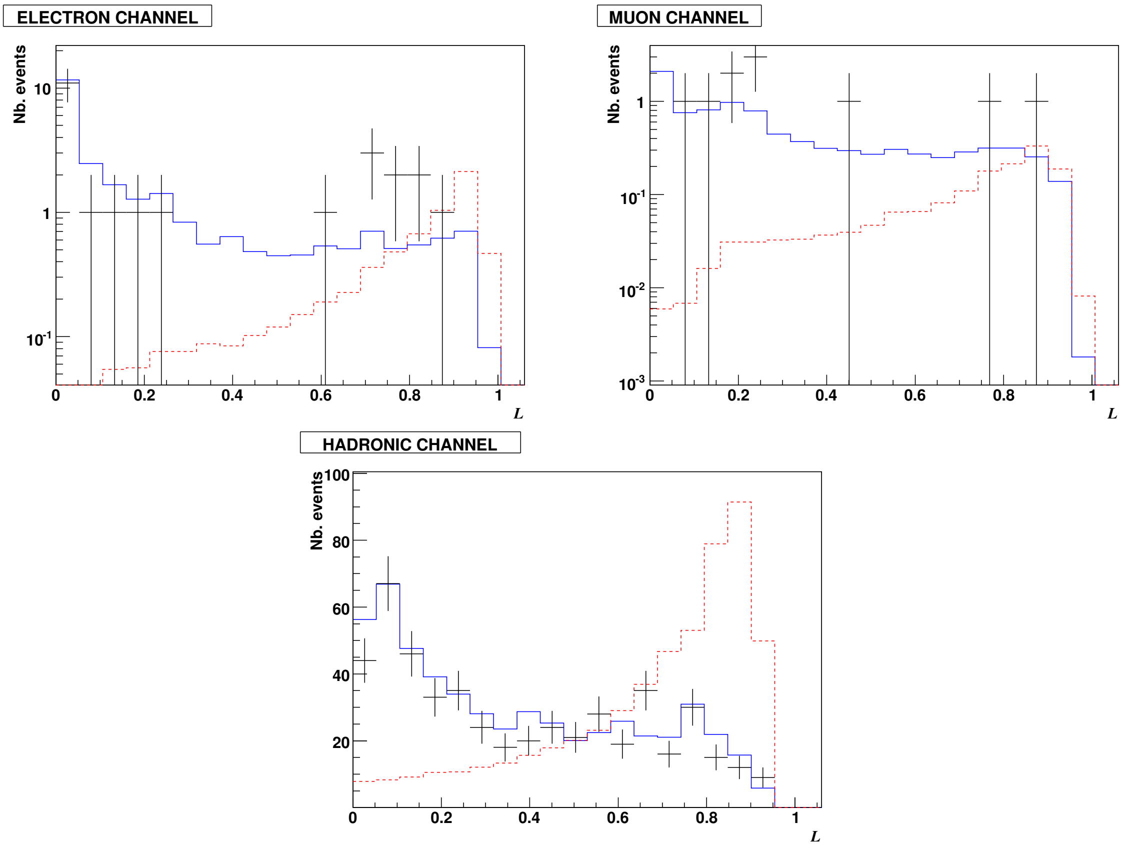

Figure 7: Distributions of the likelihood discriminator spectra for the electron, muon, and hadronic channel. In order to see the shape of the signal (red dashed histogram), it is normalized to the background.

3 Statistical evaluation of the likelihood analyses

3.1 Log-likelihood method

Under the assumption that anomalous single top production exists, the fraction of top events in the data is determined using a maximum-likelihood fit to the discriminator spectra obtained in the previous section (figure 7). We perform this maximum likelihood fit for all the channels. A likelihood function L, is introduced as the product of Poisson probabilities of observing n_k data events in each bin k of the discriminator spectrum:

$$L(S|\mathbf{N_{obs}}) = \prod_{k=1}^{n_{bin}} e^{-\mu_k} \frac{\mu_k^{n_k}}{n_k!}$$

where $\mu_k = B_k + S_k$ is the sum of the signal S_k and expected background B_k in bin k. $\mathbf{N}_{obs}$ is the data vector $(n_1, ..., n_{n_{bin}})$. The signal S_k in each bin is written as product of the signal normalization S (i.e. the total number of signal events) and the signal spectrum normalized to unity $\hat{s}_k$ in order to express the likelihood as a function of the signal normalization:

$$S_k = S \cdot \hat{s}_k$$

The signal normalization which best matches the data is the one which maximizes the likelihood function (i.e. minimizes the $-2log(L)$ function). To allow an easy interpretation, we plot

$$-2\Delta log(L) = -2(log(L) - log(L)_{min})$$

as a function of S. By using the factor 2, the log-likelihood function corresponds to a χ^2 function. The position of its minimum is the best signal normalization S_{fit} corresponding to the number of signal events. The width of this function at $-2\Delta log(L) = 1$ correponds to one standard deviation on the fitted number of signal events. Then, the fitted number of signal events in each channel is translated into a cross-section for anomalous top production by dividing through the signal efficiency (ϵ_{top}), the decay branching ratio of the channel (BR) (See table 6), and the integrated luminosity ($\mathcal{L}_{tot}$) for each individual channel. Since the analysed data sets were recorded with two different ep center-of-mass energies, the obtained cross-section is valid for an effective center-of-mass energy, $\sqrt{s_{eff}}$:

$$\sigma_{eff} = \sigma(ep \rightarrow etX, \sqrt{s_{eff}}) = \frac{S_{fit}}{\epsilon_{top} \cdot BR \cdot \mathcal{L}_{tot}}$$

It is then converted into a cross-section at $\sqrt{s} = 320GeV$ using the cross-section ratio for $\sqrt{s} = 300GeV$ and $320GeV$ ($\sigma_{300}/\sigma_{320} = 0.68$):

$$\sigma_{320} = \sigma(ep \rightarrow etX, \sqrt{s} = 320GeV) = \sigma_{eff} \frac{\mathcal{L}_{tot}}{0.68 \cdot \mathcal{L}_{300} + \mathcal{L}_{320}}$$

	efficiencies	Branching ratios
Hadronic channel	42%	0.68
Muon channel	41%	0.13
Electron channel	49%	0.13

Table 6: Efficiencies and branching ratios for the different channels.

The log-likelihoods are displayed in figure 8 as functions of the parameter S. These log-likelihoods are then translated into functions of the cross-section in figure 9, according to the formulas above. Finally, the different search channels can be combined by adding their log-likelihood functions. Due to the different efficiencies and branching ratios for each channel, the combined functions are shown with respect to single top cross-section. The combinations are shown in figure 10. The results of the maximum-likelihood fits (minimum values and standard deviations) are written in table 7. We have also done this for the hadronic channel with HERA 1 data set only (see figure 11). This yields the fits $S_{fit} = 5.62^{+7.45}_{-6.43}$ and $\sigma = 0.18^{+0.24}_{-0.21}$. Which is

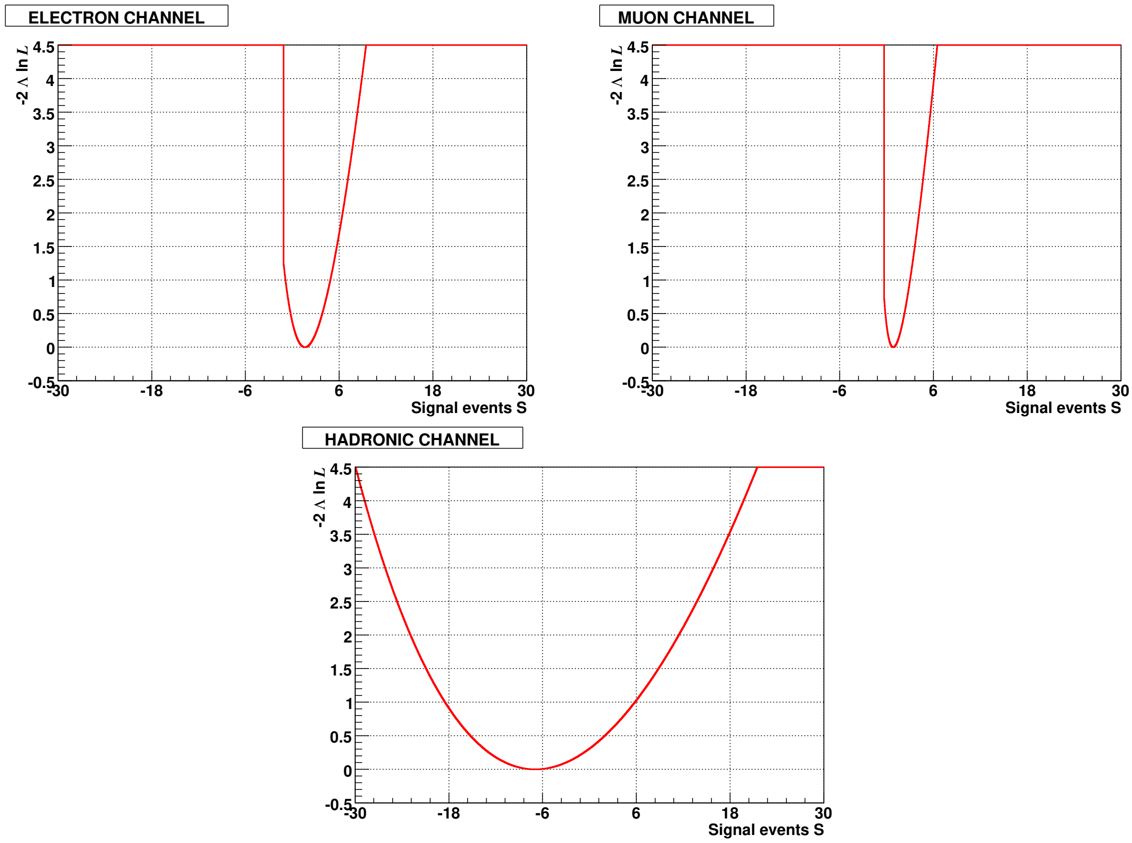

Figure 8: The log-likelihood functions of the signal fit in the electron, muon and hadronic channels. They are shown as functions of the signal normalization. ($e^{\pm}p$ Data 94-07 $486 \mathrm{pb}^{-1}$)

Max.-likelihood fit	$S \pm \delta S$	$\sigma_{320} \pm \delta\sigma_{320}$
Electron channel	$1.61^{+3.24}_{-2.50}$	$0.06^{+0.11}_{-0.09}$
Muon channel	$0.85^{+2.15}_{-1.19}$	$0.03^{+0.09}_{-0.05}$
Hadronic channel	$-6.94^{+12.74}_{-11.56}$	$-0.05^{+0.10}_{-0.09}$
El.+Mu. channels		$0.04^{+0.07}_{-0.05}$
All channels		$0.02^{+0.05}_{-0.03}$

Table 7: The number of signal events and the corresponding single top cross-section obtained by the maximum-likelihood fit. ($e^{\pm}p$ Data 94-07 $486 \mathrm{pb}^{-1}$)

quite different from the results in [1]: $S_{fit} = 1.3^{+7.8}_{-6.9}$, but still compatible within errors. Maybe it is due to different HFS algorithm and calibrations used.

Because of the small number of top candidates fitted, exclusion limits at 95% confidence level (CL) are set on the cross-section for anomalous single top production. The exclusion limits can directly be taken from the log-likelihood function. An upper bound at 95% CL correponds to a value of the log-likelihood of $-2\Delta log(L) = 2.69$. The cross-section limits for each channel

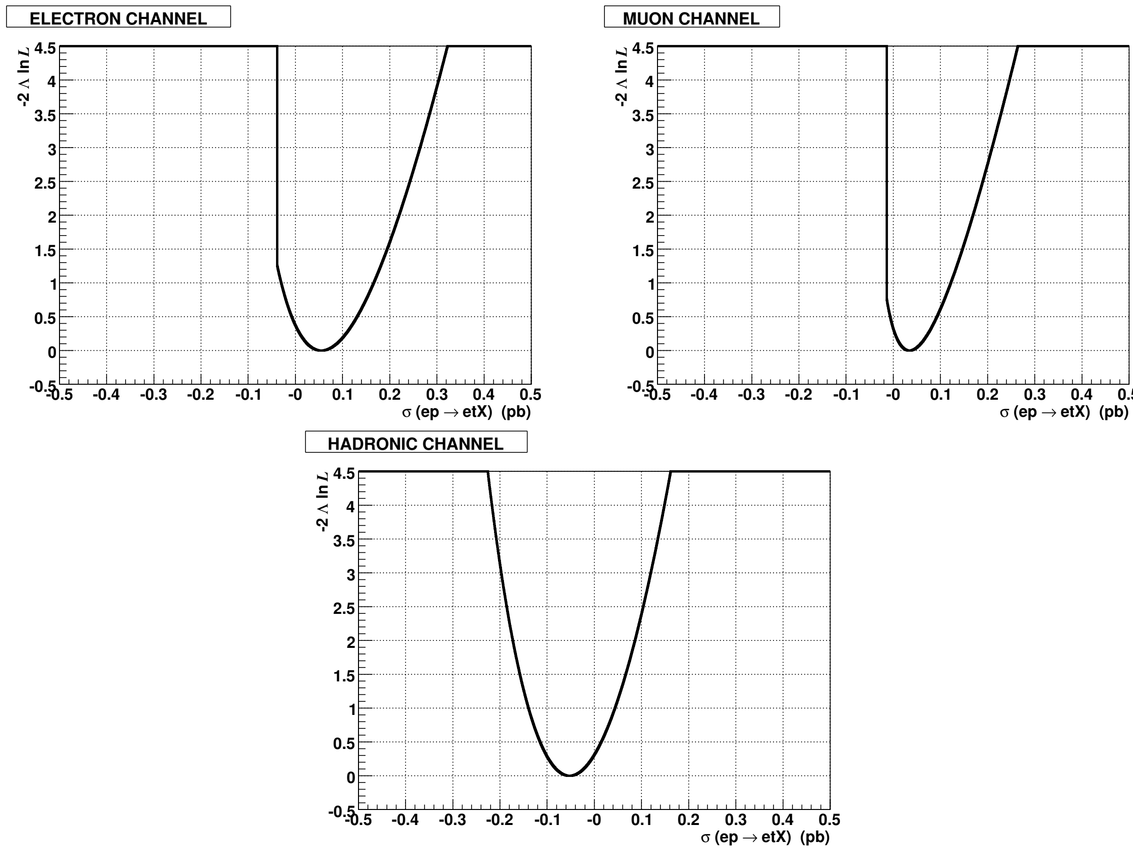

Figure 9: The log-likelihood functions of the signal fit in the electron, muon, and hadronic channels. They are shown as functions of the single top cross-section. ($e^{\pm}p$ Data 94-07 486pb^{-1})

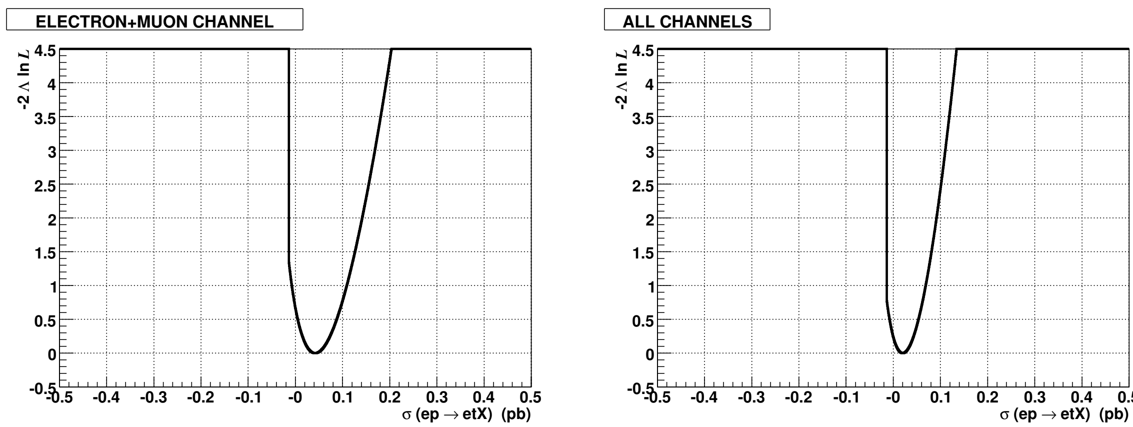

Figure 10: The log-likelihood functions of the signal for the combination of the electron and muon channels (semi-leptonic channel) and for the combination of the three channels. They are shown as functions of the single top cross-section. ($e^{\pm}p$ HERA1+2 94-07 486pb^{-1})

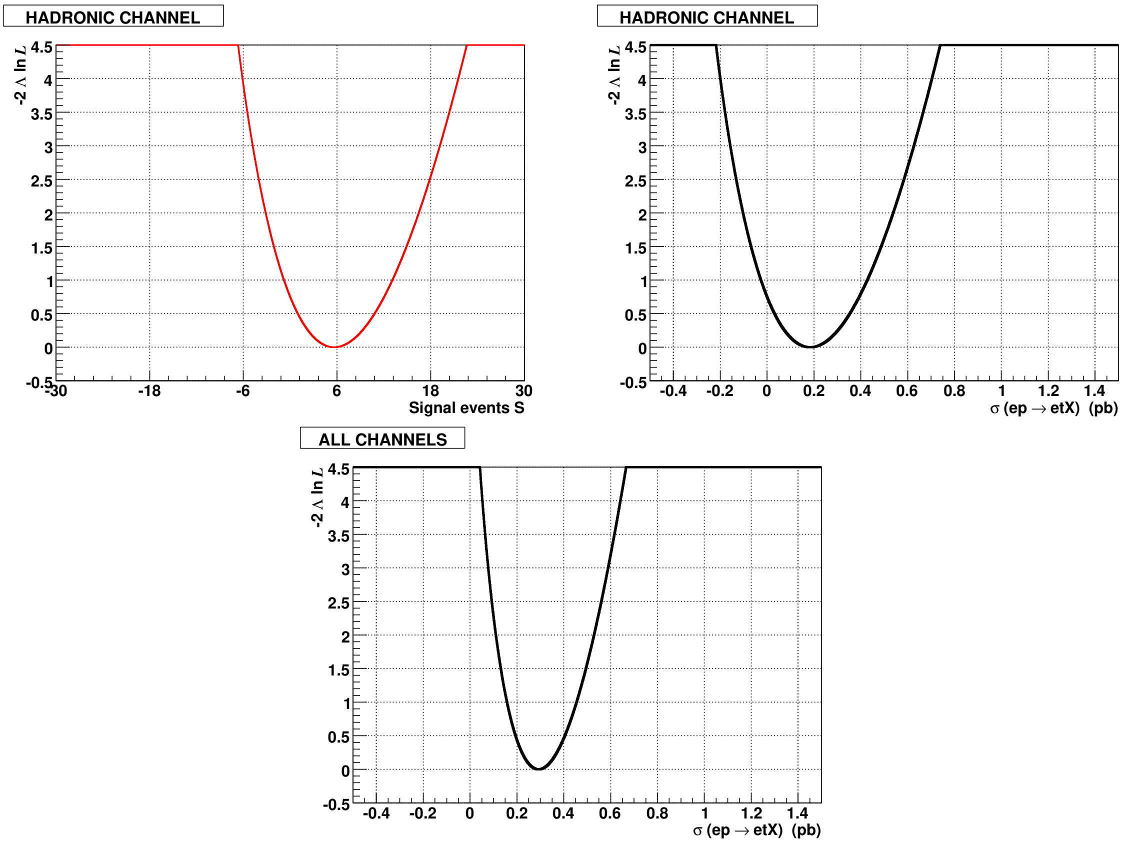

Figure 11: The log-likelihood functions of the signal fit in the hadronic channel and the combination of all the channels. They are shown as functions of the signal normalization and of the single top cross-section. ($e^{\pm}p$ HERA1 94-00 118pb^{-1})

and for the combination of these channels are shown in table 8. The limit cross-section has also been calculated in the hadronic channel with HERA 1 data only. We obtain $\sigma < 0.601\text{pb}$ at 95% CL, which has to be compared with $\sigma < 0.48\text{pb}$ at 95% CL taken from [4].

Exclusion limits on $\sigma_{320}(t \to etX)$	with $-2log(L)$	with a bayesian approach
Electron channel	< 0.251 pb	< 0.295 pb
Muon channel	< 0.197 pb	< 0.254 pb
El+Mu channel	< 0.161 pb	< 0.187 pb
Hadronic channel	< 0.110 pb	< 0.173 pb
All channels	< 0.105 pb	< 0.123 pb

Table 8: Exclusion limits at 95% CL on the single top cross-section. ($e^{\pm}p$ Data 94-07 486pb^{-1})

3.2 Bayesian approach

In the hadronic channel, there are less observed data events than events expected from the Standard Model background. Hence, the fitted number of events with this method is negative. To avoid this non-physical result, we now consider a Bayesian approach. This means that we restrict the values taken by our parameters to physical values (i.e. non-negative values) with a flat prior. Therefore, the likelihood is set to zero when the number of signal events (or the cross-section) is negative. In order to interpret it as a probability density function, we normalize this new likelihood to one. So, we obtain the density probability function, $P(\theta|\mathbf{N}_{obs})$ defined as:

$$P(\theta|\mathbf{N_{obs}}) = \frac{L(\theta|\mathbf{N_{obs}}).\pi(\theta)}{\int L(\theta|\mathbf{N_{obs}}).\pi(\theta)d\theta}$$

with

$$\pi(\theta) = \begin{cases} 0 & \theta < 0 \\ 1 & \theta \geq 0 \end{cases}$$

θ is the parameter on which the likelihood depends; it can be the number of signal events or the cross-section for anomalous single top production. $\mathbf{N}_{obs}$ is the data vector we observe. The plots P for different channels are shown in figure 13 and figure 14. In that case we combine the individual channels by multiplying the density probability functions and renormalizing the result to one. An illustration of this is shown in figure 12. The 95% CL limit, σ_{95}, is defined as:

$$\int_{\sigma_{top} \leq \sigma_{95}} P(\sigma_{top}|\mathbf{N_{obs}})d\sigma_{top} = 0.95$$

These limits on σ_{top} are shown in table 8.

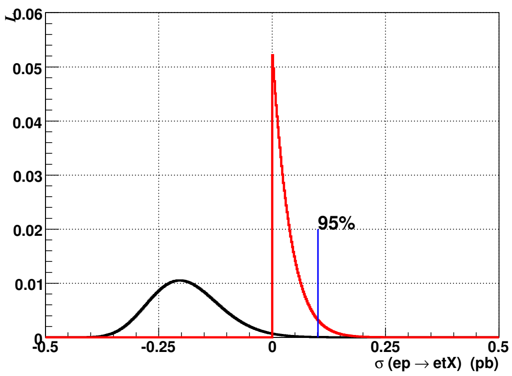

Figure 12: Illustration of how to obtain the Bayesian pdf.

In the case of both methods, we can translate the cross-section limit into an upper exclusion limit on the coupling strength of the anomalous $tu\gamma$ magnetic coupling, giving the formula:

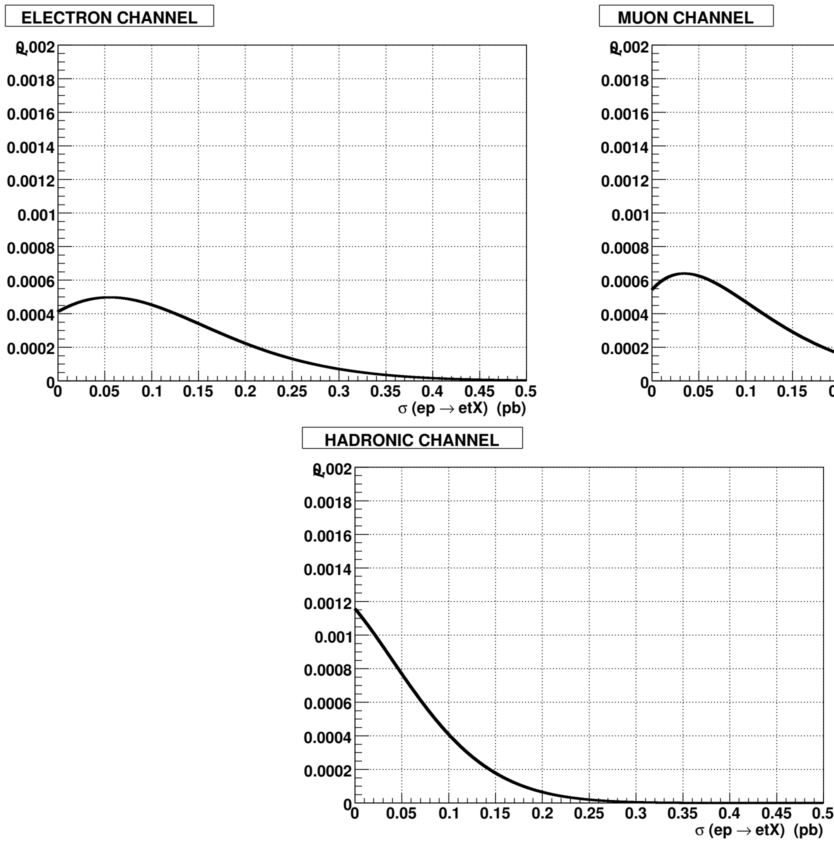

Figure 13: Probablity density functions in a bayesian approach for individual channels. They are shown as functions of the anomalous single top cross-section. ($e^{\pm}p$ Data 94-07 486pb^{-1})

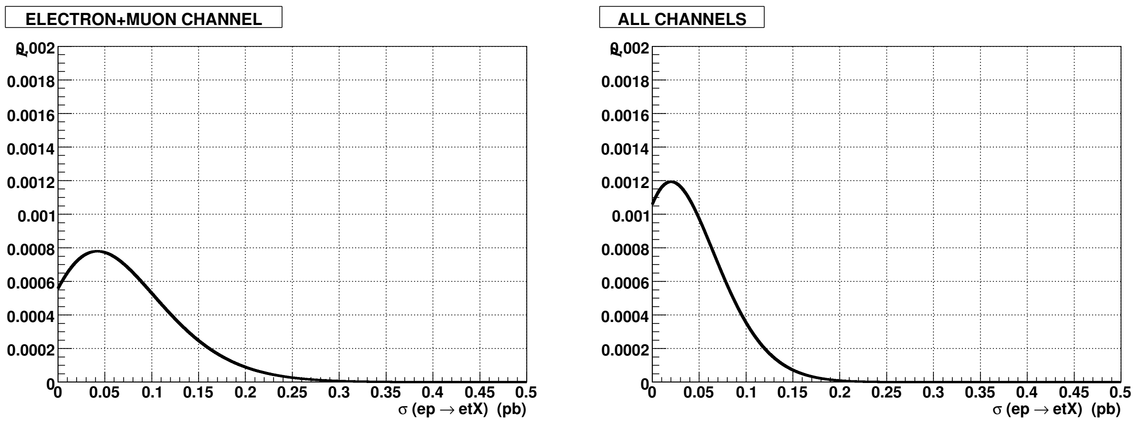

Figure 14: Probablity density functions in a bayesian approach for combined channels. They are shown as functions of the anomalous single top cross-section. ($e^{\pm}p$ Data 94-07 486pb^{-1})

$$\kappa_{tu\gamma} = \kappa_{ref}.\sqrt{\frac{\sigma_{top}}{\sigma_{ref}}}.\frac{1.5}{\sqrt{1.17}}$$

where $\kappa_{ref} = 0.1$pb, $\sigma_{ref} = 0.167$, and 1.17 is a factor to take into account NLO corrections.

Table 9 summarizes the exclusion limits obtained for each individual channel as well as for the combination of all channels and the electron+muon channel. For HERA 1 period only we find, in the hadronic channel with a log-likelihood method, a limit of $\kappa_{tu\gamma} < 0.263$ at 95% CL.

Exclusion limits on $\kappa_{tu\gamma}$	with $-2log(L)$	with a bayesian approach
Electron channel	< 0.170	< 0.184
Muon channel	< 0.151	< 0.171
El+Mu channel	< 0.136	< 0.147
Hadronic channel	< 0.112	< 0.141
All channels	< 0.110	< 0.119

Table 9: Exclusion limits at 95% CL on the $\kappa_{tu\gamma}$-coupling. ($e^{\pm}p$ Data 94-07 486pb^{-1})

4 Exclusion limits on single top production in $\kappa_{tu\gamma}$–v_{tuZ} plane

In the previous analysis, we have neglected the κ_{tuZ} coupling; this means that we have set a limit on $\kappa_{tu\gamma}$ for $v_{tuZ} = 0$ in the $\kappa_{tu\gamma}$–v_{tuZ} plane. Now, we want to obtain an exclusion limit curve in this plane. In order to set exclusion limits on the values of the effective coupling constants $\kappa_{tu\gamma}$ and v_{tuZ}, a two dimensional likelihood, L_i, is defined in the $\kappa_{tu\gamma}$–v_{tuZ} plane for each channel i as

$$L_i(N_{obs}|\kappa_{tu\gamma}, v_{tuZ}) = \frac{(N_{sig,i}(\kappa_{tu\gamma}, v_{tuZ}) + N_{SM,i})^{N_{obs,i}}.e^{-(N_{sig,i}(\kappa_{tu\gamma}, v_{tuZ})+N_{SM,i})}}{N_{obs,i}!}$$

where L_i is the probability to observe $N_{obs,i}$ events, when $N_{SM,i}$ events are expected from SM background and $N_{sig,i}$ events are expected from single top-quark production for a given pair of $\kappa_{tu\gamma}$ and v_{tuZ}. The production cross section $\sigma_{singletop}(\kappa_{tu\gamma}, v_{tuZ})$ is calculated for each pair of $\kappa_{tu\gamma}$ and v_{tuZ} (Fig. 15), using ANOTOP. The number of expected signal events , N_{sig}, is computed as:

$$N_{sig,i}(\kappa_{tu\gamma}, v_{tuZ}) = \sigma_{singletop}(\kappa_{tu\gamma}, v_{tuZ}).\epsilon_{top,i}.BR_i.\mathcal{L}_{int}$$

where:

- $\sigma_{singletop}(\kappa_{tu\gamma}, v_{tuZ})$ is the production cross section;
- $\epsilon_{top,i}$ is the selection efficiency of the channel;
- BR_i is the branching ratio of the channel;
- $\mathcal{L}_{int}$ is the integrated luminosity;

A two dimensional probability density for all the channels in the $\kappa_{tu\gamma}$–v_{tuZ} plane (see figure 16) is obtained using a Bayesian approach :

$$P(N_{obs}|\kappa_{tu\gamma}, v_{tuZ}) = \frac{\prod_i L_i(N_{obs,i}|\kappa_{tu\gamma}, v_{tuZ})}{\int_0^\infty \int_0^\infty \prod_i L_i(N_{obs,i}|\kappa_{tu\gamma}, v_{tuZ}) d\kappa_{tu\gamma} dv_{tuZ}}$$

The 95% CL limit in the $\kappa_{tu\gamma}$–v_{tuZ} plane is defined as the set of points $P(N_{obs}|\kappa_{tu\gamma}, v_{tuZ}) = P_0$ (see figure 17), for which the following relation holds:

$$\int_{P(N_{obs}|\kappa_{tu\gamma}, v_{tuZ}) > P_0} P(N_{obs}|\kappa_{tu\gamma}, v_{tuZ}) d\kappa_{tu\gamma} dv_{tuZ} = 0.95$$

We can see in table 10 the 95% CL limits set on the $\kappa_{tu\gamma}$ and the v_{tuZ} axis for each individual channels and for the combination of the channels.

We want to compare this method with the method presented in section 3.2. Therefore, we do the same thing as before, but on the $\kappa_{tu\gamma}$ and v_{tuZ} axis only; this means that $v_{tuZ} = 0$ or $\kappa_{tu\gamma} = 0$. In that case two 1-Dimensional probability distributions can be defined:

$$P_\kappa(N_{obs}|\kappa_{tu\gamma}) = \frac{\prod_i L_i(N_{obs,i}|\kappa_{tu\gamma}, v_{tuZ} = 0)}{\int_0^\infty \prod_i L_i(N_{obs,i}|\kappa_{tu\gamma}, v_{tuZ} = 0) d\kappa_{tu\gamma}}$$

$$P_v(N_{obs}|v_{tuZ}) = \frac{\prod_i L_i(N_{obs,i}|\kappa_{tu\gamma} = 0, v_{tuZ})}{\int_0^\infty \prod_i L_i(N_{obs,i}|\kappa_{tu\gamma} = 0, v_{tuZ}) dv_{tuZ}}$$

The 95% CL limits κ_{95} and v_{95} on $\kappa_{tu\gamma}$ and v_{tuZ} respectively are defined as:

$$\int_{\kappa_{tu\gamma} \leq \kappa_{95}} P_\kappa(N_{obs}|\kappa_{tu\gamma}) d\kappa_{tu\gamma} = 0.95$$

$$\int_{v_{tuZ} \leq v_{95}} P_v(N_{obs}|v_{tuZ}) dv_{tuZ} = 0.95$$

All the results are summarized in table 10. We can see that results with the 2-Dimensional method are always worse than the results obtained with 1-Dimensional method. Now, if we compare the results obtained with the 1-Dimensional method with the results in table 9 obtained with the bayesian method in section 3.2, we see a good agreement between the two methods.

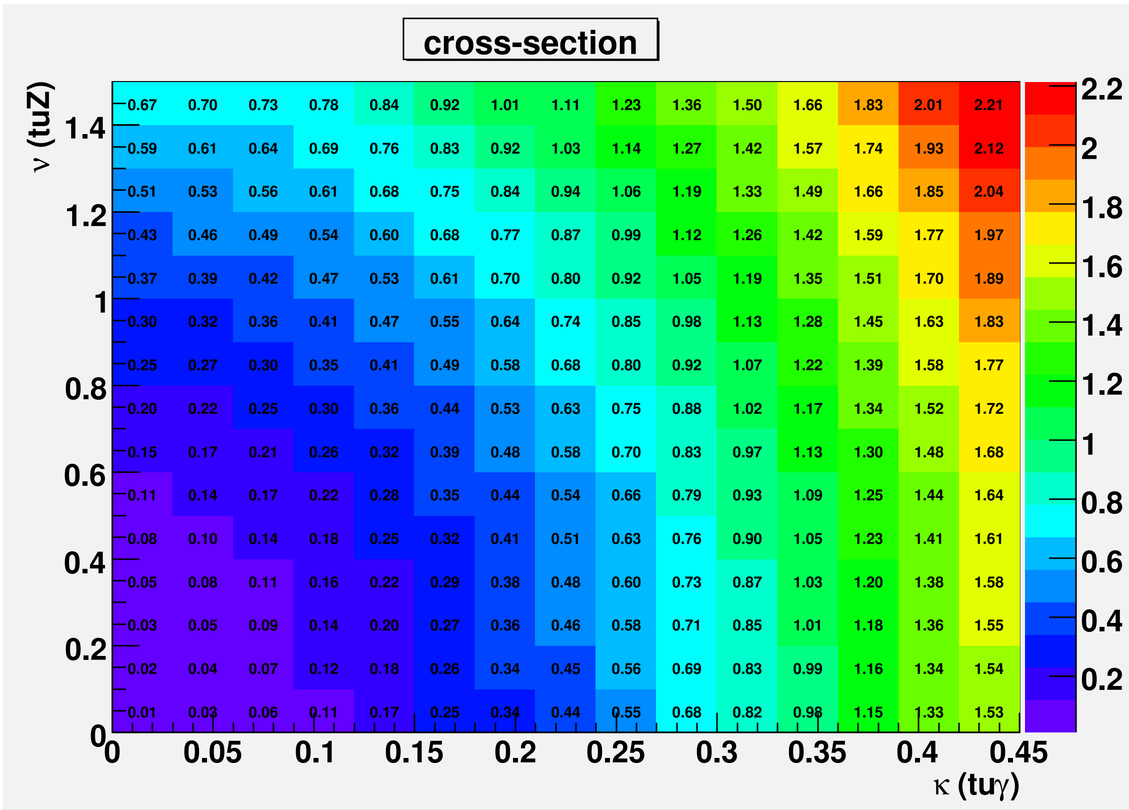

Figure 15: Cross-section for single top-quark production $ep \to etX$ as a function of the coupling constants $\kappa_{tu\gamma}$ and v_{tuZ} obtained with ANOTOP.

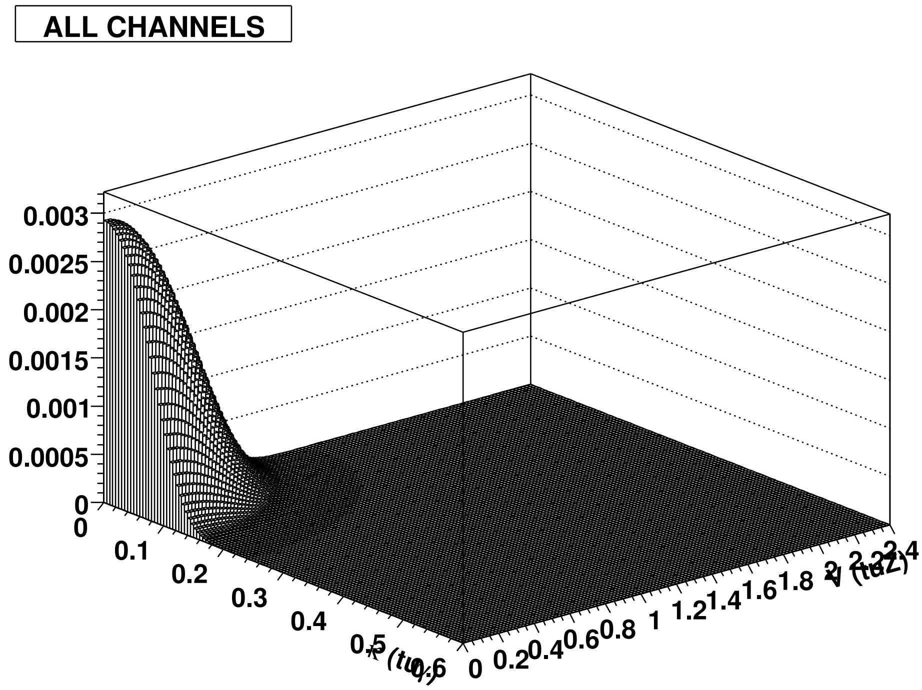

Figure 16: 2-Dimensional likelihood for the combination of all the channels. It is represented as a function of $\kappa_{tu\gamma}$ and v_{tuZ} couplings.

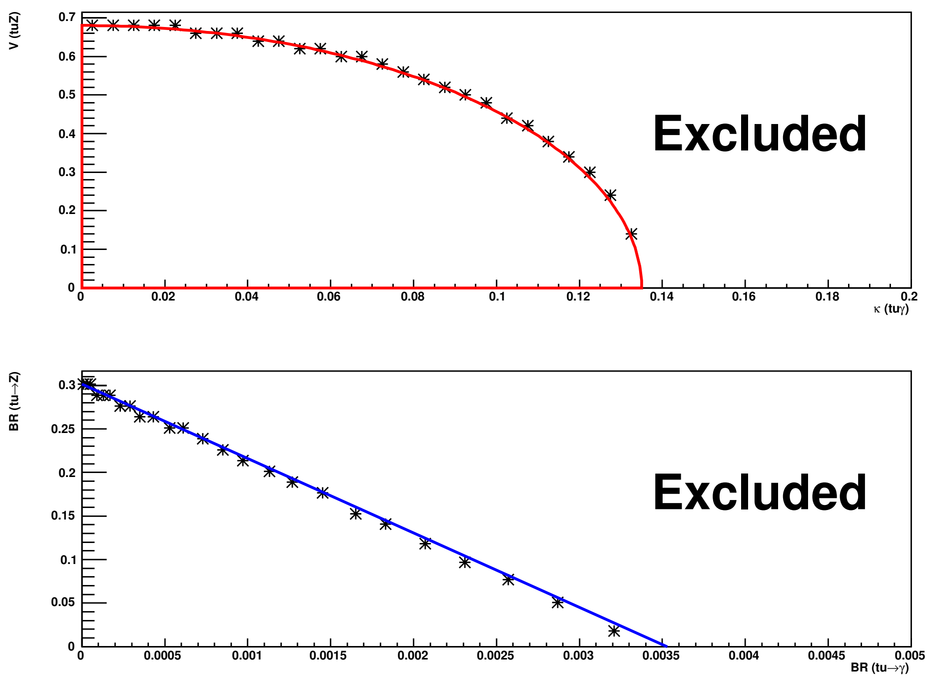

Figure 17: Exclusion limits in both $\kappa_{tu\gamma}$–v_{tuZ} and $BR(tu \to \gamma)$–$BR(tu \to Z)$ planes.

Exclusion limits	method	$\kappa_{tu\gamma}$	v_{tuZ}
Electron channel	2-dim	< 0.215	< 1.080
	1-dim	< 0.185	< 0.920
Muon channel	2-dim	< 0.215	< 1.080
	1-dim	< 0.185	< 0.940
El+Mu channel	2-dim	< 0.175	< 0.880
	1-dim	< 0.150	< 0.760
Hadronic channel	2-dim	< 0.165	< 0.840
	1-dim	< 0.135	< 0.680
All channels	2-dim	< 0.135	< 0.680
	1-dim	< 0.115	< 0.580

Table 10: Exclusion limits at 95% CL on $\kappa_{tu\gamma}$ when $v_{tuZ} = 0$ ($\kappa_{tu\gamma}$ axis) and on v_{tuZ} when $\kappa_{tu\gamma} = 0$ (v_{tuZ} axis).

We also have converted these limits into branching ratios ($BR(t \to u\gamma)$ and $BR(t \to uZ)$), thanks to the decay widths which can be parametrised as functions of $\kappa_{tu\gamma}$ and v_{tuZ} (See [6] page 36):

$$BR(t \to bW^+) = \frac{\Gamma_{t\to bW^+}}{\Gamma_{t\to bW^+} + \Gamma_{t\to u\gamma} + \Gamma_{t\to uZ}}$$

$$BR(t \to u\gamma) = \frac{\Gamma_{t\to u\gamma}}{\Gamma_{t\to bW^+} + \Gamma_{t\to u\gamma} + \Gamma_{t\to uZ}}$$

$$BR(t \to uZ) = \frac{\Gamma_{t\to uZ}}{\Gamma_{t\to bW^+} + \Gamma_{t\to u\gamma} + \Gamma_{t\to uZ}}$$

the decay widths are parametrised as follow using the coefficients shown in table 11:

$$\Gamma_{t\to bW^+} = w_{SM}$$
$$\Gamma_{t\to u\gamma} = w_\gamma.\kappa^2_{tu\gamma}$$
$$\Gamma_{t\to uZ} = w_Z.v^2_{tuZ}$$

w_{SM} (MeV)	1554
w_γ (MeV)	302
w_Z (MeV)	1449

Table 11: Values of the top decay width coefficients.

Exclusion limits	$BR(tu \to \gamma)$	$BR(tu \to Z)$
Electron channel	< 0.0089	< 0.521
Muon channel	< 0.0089	< 0.521
El+Mu channel	< 0.0059	< 0.419
Hadronic channel	< 0.0053	< 0.397
All channels	< 0.0035	< 0.301

Table 12: Exclusion limits at 95% CL on $BR(t \to u\gamma)$ and on $BR(t \to uZ)$.

5 Summary and Outlook

A search for single top production is performed using the full amount of data collected between 1994 and 2007 corresponding to a luminosity of =486pb^{-1}. In a cut-based analysis, 123 data events are selected when the prediction for Standard Model processes is 119 ± 36 events. A multivariate likelihood analysis is also performed in addition to the cut-based analysis. The top signal contribution in each channel is then determined in a maximum-likelihood fit to the likelihood discriminator distributions. For the combination of the semi-leptonic and the hadronic channel, a cross-section for single top production of $\sigma = 0.02^{+0.05}_{0.03}$ pb at $\sqrt{s} = 320$ GeV is obtained. Assuming that the small number of top candidates is a result of statistical fluctuations, exclusion limits for the single top cross-section of $\sigma < 0.123$ pb and for the anomalous coupling $\kappa_{tu\gamma} < 0.119$ are also set. Finally, we extend this analysis and set 95% CL limits in $\kappa_{tu\gamma}$–v_{tuZ} plane. Results and comparison with other experiments ([7], [8] and [6]) are shown in figure 18 and figure 19.

Some problems still have to be solved. We have to figure out why the number of events selected in HERA 1 period is not the same as in previous analyses. We also have to understand why the limits calculated in section 4 are so different in a 1-Dimensional method and in a 2-Dimensional method.

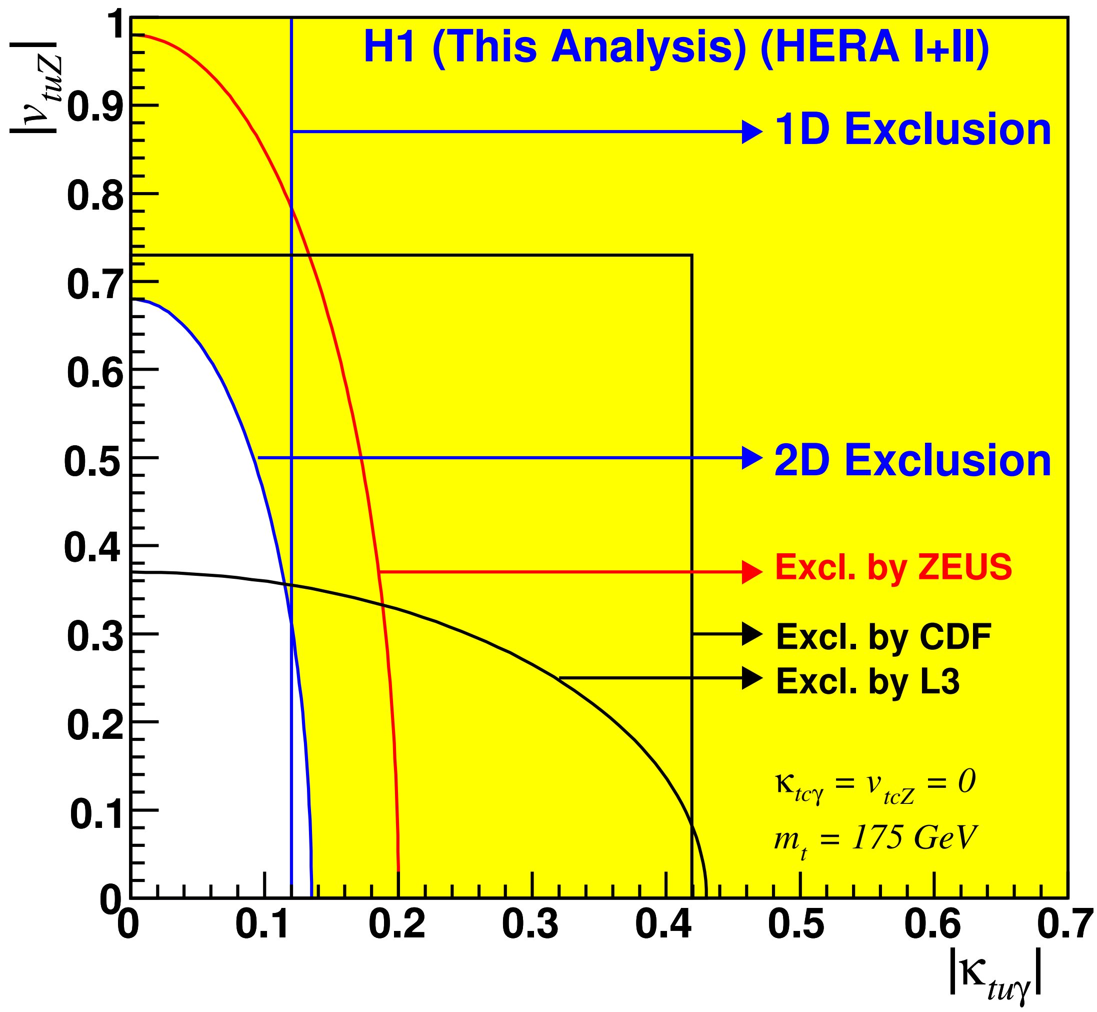

Figure 18: The current status on the anomalous magnetic coupling of the top quark to a photon and a light quark ($\kappa = \kappa_{tq\gamma}$, $q = u, c$) and on the anomalous vector coupling of the top quark to a Z boson and a light quark ($v_Z = v_{tqZ}$, $q = u, c$).

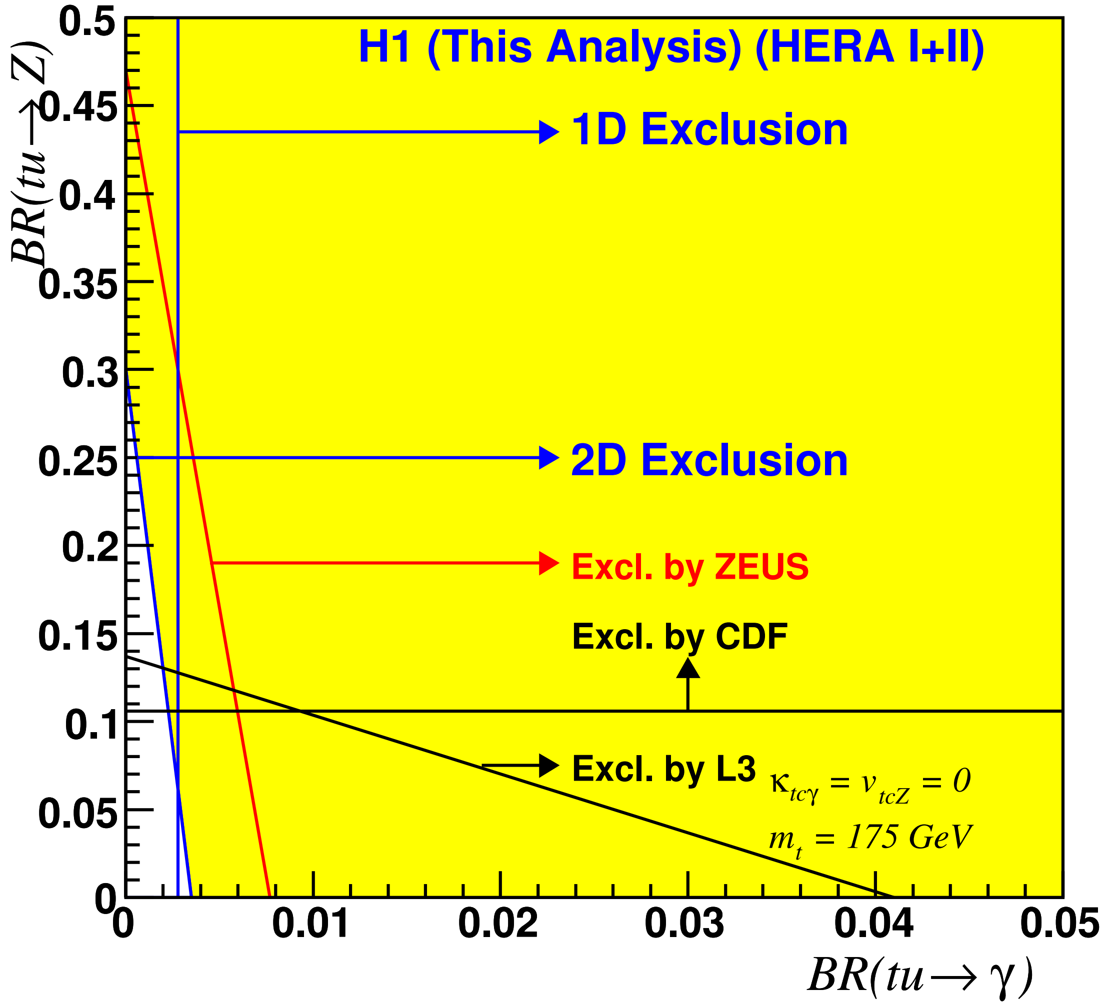

Figure 19: The current status on the branching ratios plane.

References

[1] J. Dingfelder,
Search for Anomalous Production of Single Top Quarks with the H1 Experiment at HERA,
Dissertation, Heidelberg, Germany (2003).

[2] E. Perez,
Private communication,
Hamburg, Germany (2007).

[3] H1 Collaboration,
Search for Single Top Production at HERA,
H1prelim-07-163 (2007).

[4] H1 Collaboration,
Search for Single Top Quark Production in ep *Collisions at HERA*,
Eur. Phys. (2003) [hep-ex/0310032].

[5] A. Höcker, P. Speckmayer, J. Stelzer, F. Tegenfeldt, H. Voss, K. Voss,
TMVA, Toolkit for Multivariate Data Analysis with ROOT,
CERN-OPEN-2007-007 (2007).

[6] D. Dannheim,
Search for Events with Isolated Leptons and Large Missing Transverse Momentum in ep *Collisions at HERA*,
Dissertation, Hamburg, Germany (2003).

[7] CDF Collaboration,
Search for the Flavor Changing Neutral Current Decay $t \to Zq$ *in* $p\bar{p}$ *Collisions at* $\sqrt{s} = 1.96$ *TeV*,
Preliminary Result for Summer Conferences 2007.

[8] L3 Collaboration,
Search for Single Top Production at LEP,
Phys. Lett. (2002) [hep-ex/0210041].